



Finite Element Analysis of Functionally Graded Beams using Different Beam Theories

Farshad Rahmani ^a, Reza Kamgar ^{b*}, Reza Rahgozar ^a

^a Department of Civil Engineering, Shahid Bahonar University of Kerman, Kerman, Iran.

^b Department of Civil Engineering, Shahrekord University, Shahrekord, Iran.

Received 08 July 2020; Accepted 11 October 2020

Abstract

The present study deals with buckling, free vibration, and bending analysis of Functionally Graded (FG) and porous FG beams based on various beam theories. Equation of motion and boundary conditions are derived from Hamilton's principle, and the finite element method is adopted to solve problems numerically. The FG beams are graded through the thickness direction, and the material distribution is controlled by power-law volume fraction. The effects of the different values of the power-law index, porosity exponent, and different boundary conditions on bending, natural frequencies and buckling characteristics are also studied. A new function is introduced to approximate the transverse shear strain in higher-order shear deformation theory. Furthermore, shifting the position of the neutral axis is taken into account. The results obtained numerically are validated with results obtained from ANSYS and those available in the previous work. The results of this study specify the crucial role of slenderness ratio, material distribution, and porosity condition on the characteristic of FG beams. The deflection results obtained by the proposed function have a maximum of six percent difference when the results are compared with ANSYS. It also has better results in comparison with the Reddy formulae, especially when the beam becomes slender.

Keywords: Functionally Graded Materials; Finite Element Method; Buckling Analysis; Free Vibration.

1. Introduction

A composite material is made of two or more constituent material with different mechanical properties. This new material has physical and chemical characteristics, unlike that of the individual components. In laminate composite structures, isotropic elastic layers are joined together to provide mechanical and advanced material properties. The typical problem with laminate composite is the concentration of stress at the site of separation of the different layers, which causes cracks and the delamination phenomenon. In functionally graded materials (FGMs), because the changes from one material to another are trivial, there is no delamination [1]. FGMs are categorized as composite materials that have contiguous conversion in the properties of materials from one plane to another, thus reducing the stress concentration existed in conventional composites [2]. FGMs have several potential advantages that made their use more common in comparison with laminated composites [3]. These advantages are including reducing in-plane and transverse stresses along with thickness, proportional distribution of residual stress, improved thermal properties, greater fracture and corrosion resistance, and reducing stress concentration factors [1]. These features have led to their widespread use in various scientific and engineering applications, such as mechanical, structural, aerospace, nuclear, armory and, etc. FGMs are typically made of isotropic components (e.g., metals and ceramics). FGMs are also used as

* Corresponding author: kamgar@sku.ac.ir

 <http://dx.doi.org/10.28991/cej-2020-03091604>



© 2020 by the authors. Licensee C.E.J, Tehran, Iran. This article is an open access article distributed under the terms and conditions of the Creative Commons Attribution (CC-BY) license (<http://creativecommons.org/licenses/by/4.0/>).

thermal barrier structures in environments with high thermal inclinations (e.g., gas turbine blades) [4]. In such applications, the ceramic provides heat and corrosion resistance, and metal provides strength and toughness. Porous FGMs (PFGMs) are a new class of FGMs that have been used widely in various areas of engineering and science. The wide application of porous FGMs in engineering fields is due to their rigidity-weight ratio, which makes them extremely attractive [5].

Functionally graded (FG) beams as structural elements have various applications; therefore, knowing their static and dynamic characteristic is extremely important for engineers. Various beam theories have been developed for studying the behaviour of FG beams. The simplest beam theory is the Euler-Bernoulli beam theory (EBBT), also called Classical Beam Theory (CBT). The EBT ignored the transverse shear deformation effect; therefore, the results of this theory are so inaccurate and suitable for slender beams [6]. The First-order Shear Deformation Theory (FSDT) has been developed to assume the effect of the transverse shear deformation effect. In the FSDT, the free stress boundary condition has been estimated by a shear correction factor. The Higher-order Shear Deformation (HSDT) theories have been developed to predict the behaviour of FG beams accurately. In these theories, the transverse shear deformation is approximated by a function [7, 8]. Various higher-order functions have been proposed [9].

Plenty of research has been done to study the mechanical behaviour of FG and PFG beams. In 2001, Sankar, investigated an elasticity solution for simply supported FG beams under sinusoidal load [10]. In 2011, Alshorbagy et al. [6] studied the free vibration of the Euler-Bernoulli FG beam. Eltaher et al. (2013) [11], investigated the natural frequency of FG nano beams by considering the effect of the position of the neutral axis. In 2013, Li et al. [12], exploited the relationship between buckling loads of Timoshenko FG beams and isotropic Euler-Bernoulli beam theory. Lee et al. [13], used the transfer matrix for studying the free vibration of FG beams using the Euler-Bernoulli beam theory. In 2015, Simsek, [14], investigated the vibration characteristic of bi-directional Timoshenko FG beams by assuming various boundary conditions. Jing et al. [15] exploited the static and free vibration characteristic of FG beams by coupling the Timoshenko beam theory and the Finite volume method. In 2017, the finite element method (FEM) was used by Kehya and Turan (2016) [8] for investigating the buckling and free vibration of FG beams using first-order shear deformation theory. Simsek (2010) [9] investigated the natural frequency of FG beams by using various higher-order shear deformation theories. Pradhan [16] studied the free vibration behaviour of FG beams by assuming various shear deformation theory. Giunta et al. [17] were used the meshless method for studying the bending characteristics of three-dimensional FG beams. Frikha et al. (2016) [18] introduced a new higher-order mixed beam element for bending analysis of FG beams. Xia *et al.* (2019) [2] investigated the relationship between static behaviour of FG Reddy-Bickford beams and homogenous classical beams. Patil [19] studied the vibration of FG beams using the differential quadrature method. In 2020, Pham et al. [20] investigated semi-rigid connections in FG structures using the fuzzy static finite element method. Beam elements have been helpful in solving a large number of engineering problems. Several beam theories exist to analyze the structural behaviour of slender bodies such as columns, arches, blades, aircraft wings, and bridges. The demand and application of FG beams are increasing nowadays. FGMs in the form of a beam or beam-like structures are widely used in engineering applications such as wind turbine blades. Therefore, knowing their mechanical characteristic is crucial for engineers [21]. It should be noted that a lot of engineering problems have been solved in the form of beam-like structures [22-24].

The present work deals with the study of static, buckling, and free vibration characteristic of unidirectional FG beams and porous FG beams. Hamilton's principle is used to obtain the equations of motion and the essential boundary conditions for different beam theories. The FEM is used for numerical solving of various FG and PFG beam problems. FGM and PFGM beams for the various parameters like length to thickness ratio, power-law and porosity index, and boundary conditions are studied. The accuracy and effectiveness of this paper are verified by a comparison between the results obtained by ANSYS software and those available in previous research. A SOLID-186 element having three degrees of freedom per node has been employed in the ANSYS software. The functionally graded material beam with a uniform variation of the material property through the thickness is estimated as a laminated section containing a number of isotropic layers. The power law is used to determine material properties in each layer. Ten by forty mesh and twenty number of layers are found to give good accuracy from convergence studies. As a part of this study, a new polynomial function is introduced to approximate the shear strain. In the previous study, the effect of the neutral axis position is not significant for various analyses. Moreover, the effect of the power-law index on the shear correction factor is not considered for different analyses, including bending, free vibration, and buckling.

2. Mathematics and Formulation

2.1. Constitutive Relation

Various prevalent methods are existed methods for acquiring the effective mechanical properties of materials. These methods are the rule of mixture, the Murray-Tanaka method, and Hill's own adaptive approach [25]. In the present paper, the rule of the mixture is used to obtain the effective material properties.

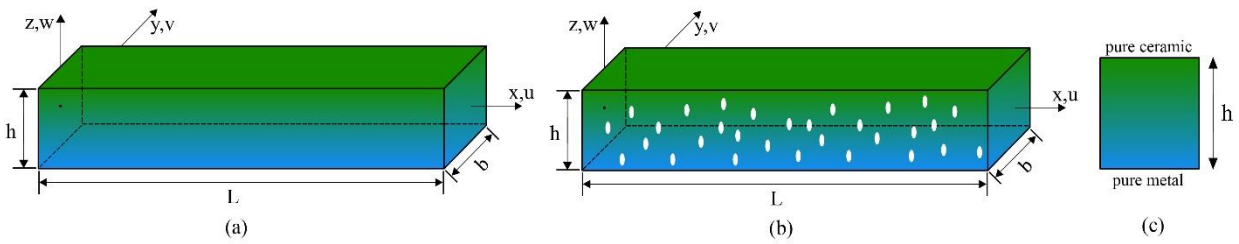


Figure 1. (a) Geometry and coordinates in FG beams, (b) General coordinates and material gradation in porous FG beams, (c) Cross-section and material gradation in FG beams

Where \$L\$, \$h\$ and \$b\$ are the length, the height, and width of the beam, respectively.

2.2. Rule of Mixture

In Figure 1, it can be seen a general FGM beam, which is made of two different materials (e.g., steel and ceramic), in which the mechanical properties are changing smoothly through the thickness. In Figure 2-a, the effect of the various power-law index is shown. According to the power-law distribution, mechanical properties of the FG beam can be defined as:

$$F_{fgm}(z) = f_b + (f_u - f_b) \times V_u, \quad V_u = \left(\frac{z}{h} + \frac{1}{2}\right)^n \quad \text{and} \quad V_b = 1 - V_u \tag{1.a}$$

$$F_{fgm}(z) = f_b + (f_u - f_b) \times V_p$$

$$V_p = \left(\frac{z}{h} + \frac{1}{2}\right)^n - \left(\frac{\alpha}{2}\right)(f_u + f_b) \quad \text{where} \quad 0 \leq \alpha \leq 1 \tag{1.b}$$

Where; \$f_b, f_t\$ show the material properties of the beam at the bottom and the upper face of the beam. Also, the parameter \$n\$ depicts the non-negative power-law index, which relates to the distribution of material properties along with the thickness of the beam. The component \$V_u, V_b\$ and \$V_p\$ are the volume fraction of the upper and lower surfaces and porous media, respectively. \$\alpha\$ indicates the porosity condition in which \$\alpha = 0\$ means there is no porosity. The distribution of porous FGMs for various \$\alpha\$ is shown in Figure 2-b.

3. Kinematic

Consider a beam in Figure 1, a global coordinate system is assumed, the \$x\$-coordinate coincide with the beam axis, \$z\$-coordinate is taken along the thickness, and \$y\$-coordinate is along the width of the beam. The displacement field of the beam can be expressed as follows based on different theories:

3.1. Euler-Bernoulli Beam Theory (EBBT)

The governing displacement equation of Euler-Bernoulli beam with 3 degrees of freedom per node is given by:

$$U(x, z, t) = u_0(x, t) - z \frac{\partial w_0(x, t)}{\partial x} \tag{2}$$

$$W(x, z, t) = w_0(x, t)$$

Displacement field equation in matrix form is:

$$\begin{pmatrix} U \\ W \end{pmatrix} = \begin{bmatrix} 1 & 0 & -z \\ 0 & 1 & 0 \end{bmatrix} \{u_0 \quad w_0 \quad w_{0,x}\}^T = [z_d] \{d\} \tag{3}$$

Using Equation 2, the strain field equation can compute as bellow:

$$\epsilon_{xx} = \frac{\partial U}{\partial x} = \frac{\partial u_0}{\partial x} - \frac{\partial^2 w_0}{\partial x^2} = \epsilon_{xx}^0 - z \epsilon_{xx}^3 \tag{4}$$

$$\epsilon_{xx} = [1 \quad -z] \{ \epsilon_{xx}^0, \epsilon_{xx}^3 \}^T = [z_\epsilon] [\hat{\epsilon}]$$

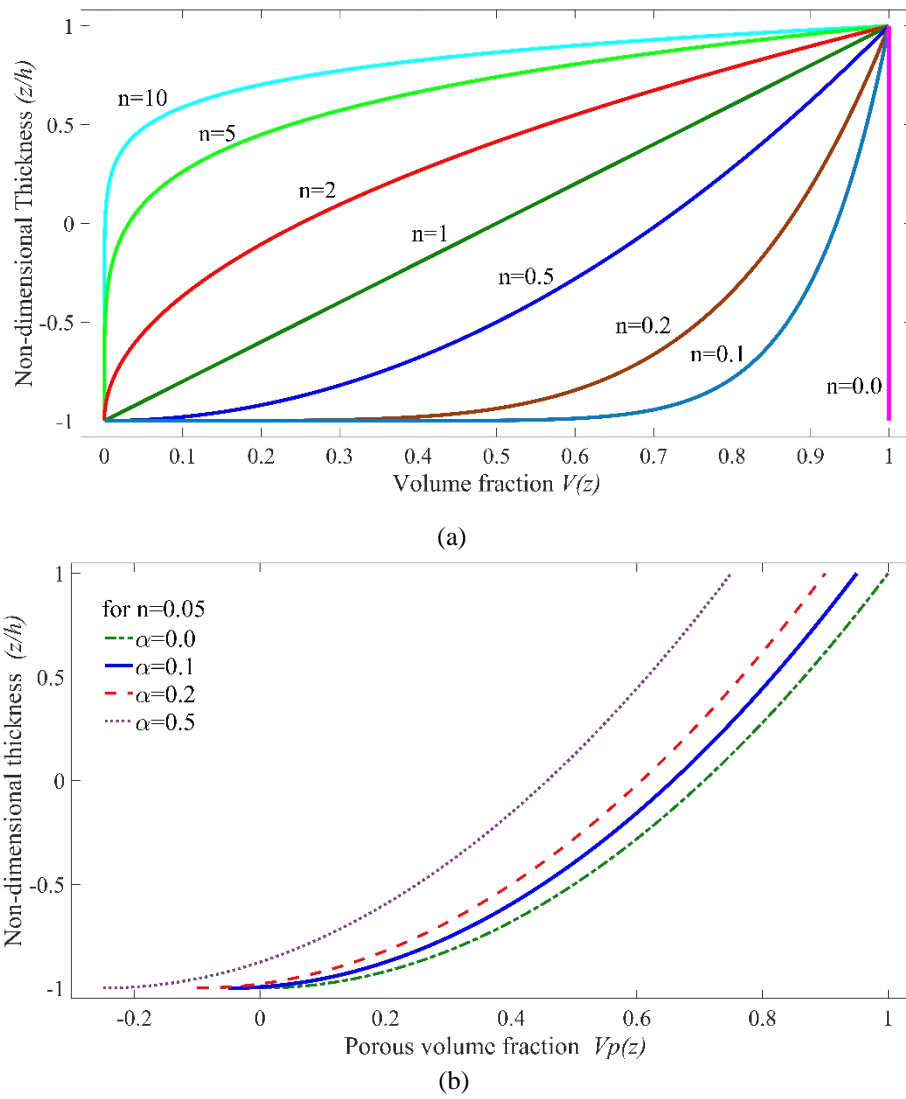


Figure 2. (a) Volume fraction vision along with the thickness (b) The effect of porosity on the volume fraction

By assuming Hook’s law, the strain-stress relationship describes as below:

$$\sigma_{xx} = E(z)\varepsilon_{xx} = E(z)[z_\varepsilon][\hat{\varepsilon}] \tag{5}$$

$$\hat{\sigma} = \begin{Bmatrix} N \\ M \end{Bmatrix} = \iint_A \begin{Bmatrix} \sigma_{xx} \\ -z\sigma_{xx} \end{Bmatrix} dA = \iint_A [z_\varepsilon]^T \sigma dA \tag{6}$$

Using Hamilton’s principle and applying the variational method to Equations 3 and 5, the general displacement field of the beam is:

$$\int_{t_1}^{t_2} (\delta S - \delta K + \delta V) dt$$

$$\delta S = \iiint_v \delta \hat{\varepsilon}^T \sigma dV = \int_l \delta \hat{\varepsilon}^T \left(\iint_A [z_\varepsilon]^T D [z_\varepsilon] dA \right) \hat{\varepsilon} dx = \int_l \delta \hat{\varepsilon}^T \hat{D} \hat{\varepsilon} dx \tag{7}$$

$$\delta K = \frac{1}{2} \iiint_v \rho(z) \delta \dot{u}^T \dot{u} dV = \int_l \delta \dot{u}^T \left(\iint_A [z_d]^T \rho(z) [z_d] dA \right) \dot{u} dx$$

$$\delta V = \iiint_v \delta u^T f_b dv + \iint_A \delta u^T q_s + u^T p$$

Where δS , δK and δV are strain energy, kinetic energy, and work done by external forces, respectively.

The constitutive matrix $[\hat{D}]$ and inertia matrix $[\hat{\rho}]$ is given by:

$$\hat{D} = \iint_A [z_\varepsilon]^T \begin{bmatrix} E(z) & 0 \\ 0 & G(z) \end{bmatrix} [z_\varepsilon] dA = \begin{bmatrix} D11 & D12 \\ D12 & D22 \end{bmatrix}$$

$$(D11, D12, D22) = \iint_A (1, -z, z^2) E(z) dA$$

$$[\hat{\rho}] = \iint_A [z_d]^T \rho [z_d] dA = \begin{bmatrix} I_1 & 0 & I_2 \\ 0 & I_1 & 0 \\ I_2 & 0 & I_3 \end{bmatrix} \tag{8}$$

$$(I_1, I_2, I_3) = \iint_A (1, -z, z^2) \rho(z) dA$$

3.2. First-order Shear Deformation Beam Theory (FSDBT)

The axial and transverse displacement equations of a FG beam with three degrees of freedom per node based on First-order shear deformation theory are expressed as:

$$U(x, z, t) = u_0(x, t) - z\psi_x \tag{9.a}$$

$$W(x, z, t) = w_0(x, t)$$

Displacement field equation in the matrix form:

$$\begin{pmatrix} U \\ W \end{pmatrix} = \begin{bmatrix} 1 & 0 & -z \\ 0 & 1 & 0 \end{bmatrix} \{u_0 \quad w_0 \quad \psi_x\}^T = [z_d] \{d\} \tag{9.b}$$

Using Equation 9.a, the only non-zeros strain-displacement field equations are given by:

$$\varepsilon_{xx} = \frac{\partial U}{\partial x} = \frac{\partial u_0}{\partial x} - \frac{\partial \psi_x}{\partial x} = \varepsilon_{xx}^0 - z\varepsilon_{xx}^1$$

$$\gamma_{xz} = \frac{\partial U}{\partial z} + \frac{\partial W}{\partial x} = \left(\frac{\partial w_0}{\partial x} - \psi\right) = \kappa_{xz}^0 \tag{10}$$

$$\varepsilon_{xx} = \begin{bmatrix} 1 & -z & 0 \\ 0 & 0 & 1 \end{bmatrix} \{\varepsilon_{xx}^0, \varepsilon_{xx}^1, \kappa_{xz}^0\}^T = [z_\varepsilon] [\hat{\varepsilon}]$$

By considering Hook’s law, and using Equation 9.a, the stress field equation describes as below:

$$\sigma_{xx} = E(z)\varepsilon_{xx} = E(z)(\varepsilon_{xx}^0 - z\varepsilon_{xx}^1)$$

$$\tau_{xz} = G(z)\gamma_{xz} = \kappa G(z)(\kappa_{xz}^0) \tag{11}$$

$$\hat{\sigma} = \begin{Bmatrix} N \\ M \\ Q \end{Bmatrix} = \iint_A \begin{Bmatrix} \sigma_{xx} \\ -z\sigma_{xx} \\ \tau_{xz} \end{Bmatrix} dA = \iint_A [z_\varepsilon]^T \sigma dA \tag{12}$$

Where; κ is the shear correction factor, which indicates the variation of shear stress through the beam thickness. In composite materials, the shear correction factor κ is not constant and depends on both the cross-section shape and the distribution of material along with the beam thickness [7]. Herein, for the sake of brevity, the mathematical formulation of the shear correction factor is neglected; therefore, for more information, the [7] can be seen. In Table 1, some shear correction factor is calculated and shown.

Table 1. The shear correction factor concerning the power-law index

n	0.0	0.2	1.0	2.0	5.0	10.0
κ	0.8333	0.8437	0.8304	0.7795	0.6783	0.6902

Applying Hamilton’s principle and variational method to Equations 10 and 11, the general displacement field of the beam is:

$$\int_{t_1}^{t_2} (\delta S - \delta K + \delta V) dt$$

$$\delta S = \iiint_v \delta \hat{\epsilon}^T \sigma dV = \int_l \delta \hat{\epsilon}^T \left(\iint_A [z_\epsilon]^T D [z_\epsilon] dA \right) \hat{\epsilon} dx = \int_l \delta \hat{\epsilon}^T \hat{D} \hat{\epsilon} dx \tag{13}$$

$$\delta K = \frac{1}{2} \iiint_v \rho(z) \delta \dot{u}^T \dot{u} dV = \int_l \delta \dot{u}^T \left(\iint_A [z_d]^T \rho(z) [z_d] dA \right) \dot{u} dx$$

$$\delta V = \iiint_v \delta u^T f_b dv + \iint_A \delta u^T q_s + u^T p$$

Where; δS , δK and δV are strain energy, kinetic energy, and work done by external forces, respectively. t_1 and t_2 are the initial and final times, respectively.

The constitutive matrix $[\hat{D}]$ and inertia matrix $[\hat{\rho}]$ is described as follow:

$$D = \iint_A [z_\epsilon]^T \begin{bmatrix} E(z) & 0 \\ 0 & \kappa G(z) \end{bmatrix} [z_\epsilon] dA = \begin{bmatrix} D11 & D12 & 0 \\ D12 & D22 & 0 \\ 0 & 0 & D33 \end{bmatrix}$$

$$(D11, D12, D22) = b \iint_A (1, -z, z^2) E(z) dA$$

$$(D33) = b \iint_A G(z) dA \tag{14}$$

$$[\hat{\rho}] = \iint_A [z_d]^T \rho [z_d] dA = \begin{bmatrix} I_1 & 0 & I_2 \\ 0 & I_1 & 0 \\ I_2 & 0 & I_3 \end{bmatrix}$$

$$(I_1, I_2, I_3) = \iint_A (1, -z, z^2) \rho(z) dA$$

3.3. Higher-order Shear Deformation Beam Theory (HSDBT)

The general displacement equations of Higher-order shear deformation beam with 4 degrees of freedom per node are given by:

$$U(x, z, t) = u_0(x, t) + z\psi_x + f(z)(\psi_x + \frac{\partial w_0}{\partial x}) \tag{15.a}$$

$$W(x, z, t) = w_0(x, t)$$

Equation 15.a can be rewritten in the matrix form as follows:

$$\begin{pmatrix} U \\ W \end{pmatrix} = \begin{bmatrix} 1 & f(z) & (z + f(z)) & 0 \\ 0 & 0 & 0 & (1 - f'(z)) \end{bmatrix} \left\{ \begin{matrix} u_0 & w_0 & \frac{\partial w_0}{\partial x} & \psi_x \end{matrix} \right\}^T = [z_d] \{d\} \tag{15.b}$$

Where; $f(z)$ is a function which approximates the shear strain through thickness. $f'(z)$ denotes the derivative of $f(z)$ with respect to the z .

Using Equation 15.a, the strain field equation of HSDT is of the form of:

$$\epsilon_{xx} = \frac{\partial U}{\partial x} = \frac{\partial u_0}{\partial x} + \frac{\partial \psi_x}{\partial x} - f(z) \left(\frac{\partial \psi_x}{\partial x} + \frac{\partial^2 w_0}{\partial x^2} \right) = \epsilon_{xx}^0 + z \epsilon_{xx}^1 - f(z) (\epsilon_{xx}^1 + \epsilon_{xx}^3)$$

$$\gamma_{xz} = \frac{\partial U}{\partial z} + \frac{\partial W}{\partial x} = \left(\frac{\partial w_0}{\partial x} + \psi \right) - f'(z) \left(\frac{\partial w_0}{\partial x} + \psi \right) = \kappa_{xz}^0 - f'(z) (\kappa_{xz}^2)$$
(16)

$$\varepsilon_{xx} = \begin{bmatrix} 1 & (z + f(z)) & f(z) & 0 \\ 0 & 1 & 0 & (1 - f'(z)) \end{bmatrix} [\hat{\varepsilon}] = [z_\varepsilon] [\hat{\varepsilon}]$$

By assuming Hook's law, and using Equation 16, the stress field equations describe as below:

$$\sigma_{xx} = E(z)\varepsilon_{xx} = E(z)(\varepsilon_{xx}^0 + z\varepsilon_{xx}^1 - f(z)(\varepsilon_{xx}^1 + \varepsilon_{xx}^3)) \tag{17}$$

$$\tau_{xz} = G(z)\gamma_{xz} = G(z)(1 - f'(z))(\kappa_{xz}^2)$$

$$\hat{\sigma} = \{N, M, P, Q, R\}^T = \iint_A \{\sigma_{xx}, -z\sigma_{xx}, -z^2\sigma_{xx}, \tau_{xz}, z\tau_{xz}\}^T dA = \iint_A [z_\varepsilon]^T \sigma dA \tag{18}$$

Using Hamilton's principle and applying the vibrational method to Equations 16 and 17, the general displacement field of the beam is:

$$\int_{t_1}^{t_2} (\delta S - \delta K + \delta V) dt$$

$$\delta S = \frac{1}{2} \iiint_v \delta \hat{\varepsilon}^T \sigma dV = \int_l \delta \hat{\varepsilon}^T \left(\iint_A [z_\varepsilon]^T D [z_\varepsilon] dA \right) \hat{\varepsilon} dx = \int_l \delta \hat{\varepsilon}^T \hat{D} \hat{\varepsilon} dx \tag{19}$$

$$\delta K = \frac{1}{2} \iiint_v \rho(z) \delta \dot{u}^T \dot{u} dV = \int_l \delta \dot{u}^T \left(\iint_A [z_d]^T \rho(z) [z_d] dA \right) \dot{u} dx$$

$$\delta V = \iiint_v \delta u^T f_b dv + \iint_A \delta u^T q_s + u^T p$$

Where; δS , δK and δV are the strain-energy, the kinetic energy, work done by axial forces, and virtual work done by an external force. t_1 and t_2 are the initial and final times, respectively.

It is useful to introduce the constitutive matrix $[\hat{D}]$ inertia matrix $[\hat{\rho}]$ are as follows:

$$D = \iint_A [z_\varepsilon]^T \begin{bmatrix} E(z) & 0 \\ 0 & G(z) \end{bmatrix} [z_\varepsilon] dA = \begin{bmatrix} D11 & D12 & D13 & 0 \\ D12 & D22 & D23 & 0 \\ D13 & D23 & D33 & 0 \\ 0 & 0 & 0 & D44 \end{bmatrix}$$

$$(D11, D12, D22, D23, D33) = b \iint_A \{1, z + f(z), f(z), (z + f(z))^2, f(z)(z + f(z)), (f(z))^2\} dA \tag{20}$$

$$(D44) = b \iint_A (1 - f'(z))^2 G(z) dA$$

$$[\hat{\rho}] = \iint_A [z_d]^T \rho [z_d] dA = \begin{bmatrix} J_1 & 0 & J_2 & J_3 \\ 0 & J_1 & 0 & 0 \\ J_2 & 0 & J_4 & J_5 \\ J_3 & 0 & J_5 & J_6 \end{bmatrix}$$

$$(J_1, J_2, J_3, J_4, J_5, J_6) = \iint_A (1, f(z), z + f(z), f(z)^2, f(z)(z + f(z)), (z + f(z))^2) \rho(z) dA$$

The shear strain function is introduced as below:

Reddy: $f(z) = \frac{-4z^3}{3h^2}$

Present: $f(z) = \frac{-11z^3}{6h^2} + \frac{6z^5}{5h^4}$ (21)

The stress-free boundary condition is satisfied on the bottom and top surface of the beam by both functions.

$$\tau_{xz}(x, \pm \frac{h}{2}) = 0 \tag{22}$$

3.4. The Position of the Neutral Axis

In FG materials, due to the variation of the mechanical properties, the position of the neutral axis is changing [11]. The effect of the power-law index and material properties is shown in Figure 3. The position of the neutral axis can be computed by using the following formulation:

$$z_0 = \frac{\int_l E(z)zdz}{\int_l E(z)dz} = \frac{nh(E_t - E_b)}{(2n + 4)(E_t + E_b)} \tag{23}$$

Where; E_b , E_t , h , n is denoting modulus of Elasticity of upper and bottom surface, the height of the beam and power-law index, respectively.

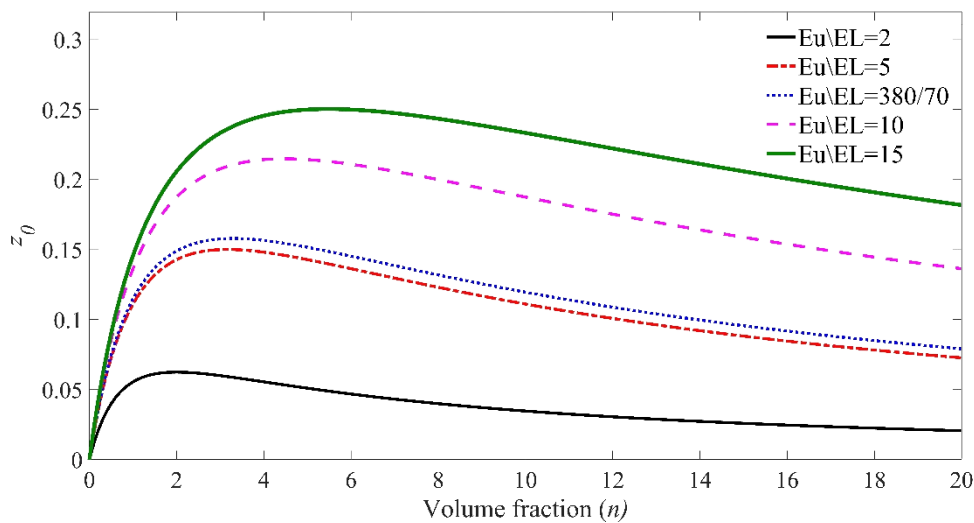


Figure 3. The effect of power-law exponent on the position of the neutral axis

4. Finite Element Formulation

There are various numerical methods used for solving engineering problems [26-28]. In the present paper, the Finite Element Method (FEM) is used to solve the governing equations. The equations of motion in the previous sections, are numerically solved by the FEM for bending, buckling, and free vibration problems. FEM formulation of each beam theories describe separately as follow:

4.1. Euler-Bernoulli Beam Theory (EBBT)

In EBBT, the Lagrange shape function approximates the in-plane displacement. Also, the Hermite cubic shape function is used for the estimation of the transverse displacement and rotation.

$$\begin{aligned} U &= \sum_{i=1}^{NE} N_i(\xi)d_{1i}^e & d_{1i}^e &= \{u_i\} \\ W &= \sum_{i=1}^{NE} H_i(\xi)d_{2i}^e & d_{2i}^e &= \{w_i, \theta_i\} \\ \varepsilon &= \sum_{i=1}^{NE} B_i d_i^e & d_i^e &= \{u_i, w_i, \theta_i\} \end{aligned} \tag{24}$$

Where; N_i and H_i are Lagrange and cubic Hermite cubic shape functions. For more information, see Alshorbagy et al. (2011) [6].

4.2. First-order Shear Deformation Beam Theory (FSDBT)

In FSDBT, the Lagrange shape function is used for both in-plane and transverse displacements and also rotation.

$$U = \begin{Bmatrix} U \\ W \\ \theta \end{Bmatrix} = \sum_{i=1}^{NE} N_i(\xi) d_i^e \quad d_i^e = \{u_i, w_i, \theta_i\} \quad (25)$$

$$\varepsilon = \sum_{i=1}^{NE} B_i d_i^e$$

4.3. Third-order Shear Deformation Beam Theory (TSDBT)

In TSDT, the Lagrange shape function estimated the in-plane displacement, and the Hermit shape function estimated the transverse displacement and rotation, respectively.

$$U = \sum_{i=1}^{NE} N_i(\xi) d_{1i}^e \quad d_{1i}^e = \{u_i\}$$

$$W = \sum_{i=1}^{NE} H_i(\xi) d_{2i}^e \quad d_{2i}^e = \left\{ w_i, \frac{dw_i}{dx}, \psi_x \right\} \quad (26)$$

$$\varepsilon = \sum_{i=1}^{NE} B_i d_i^e \quad d_i^e = \left\{ u_i, w_i, \frac{dw_i}{dx}, \psi_x \right\}$$

The element Stiffness, mass, and geometric stiffness matrix, respectively can be calculated as below:

$$[K^e] = \int_l [B]^T \hat{D} [B] dx = \int_{-1}^1 [B]^T \hat{D} [B] |J| d\xi = \sum_{i=1}^{Ng} B_i^T \hat{D} B_i |J| w_i$$

$$[M^e] = \int_l [N]^T \hat{\rho} [N] dx = \int_{-1}^1 [N]^T \hat{\rho} [N] |J| d\xi = \sum_{i=1}^{Ng} N_i^T \hat{\rho} N_i |J| w_i \quad (27)$$

$$[K_G^e] = \int_l P [N_G]^T [N_G] dx = \int_{-1}^1 P [N_G]^T [N_G] |J| d\xi = P \sum_{i=1}^{Ng} N_{Gi}^T N_{Gi} |J| w_i$$

$$N_G = \int_l \left(\frac{dw}{dx} \right)^2 dx$$

The components K^e , M^e and K_G^e denote the element stiffness, mass, and geometric stiffness matrix, respectively. Here the Gaussian quadrature is used to solve the integration. Where Ng is indicate the number of gauss points. The construction of finite element analysis is demonstrated as follows:

Structures of FEM code for FG beam analysis

- a: Read input data
 - Geometric data: (node coordinates, element connectivity, and ...)
 - Mechanical properties: (Young's modulus, Poisson ratio, and ...)
 - b: Calculating constitutive matrix
 - c: **for** loop over elements **do**
 - d: **for** loop over gauss points **do**
 - e: Calculating strain matrix [B]
 - f: Calculating element stiffness matrix $[K]^e, [kg]^e$
 - Calculating element mass matrix $[M]^e$,
 - Calculating the force matrix
 - g: **end**
 - h: Assembling the element stiffness, mass and force matrices in the global coordinate system
 - i: **end**
 - j: Applying boundary conditions
 - k: Solving equations for static, free vibration and buckling analyses
 - l: Display results
-

4.4. The Validity of New Shear Strain Function

In this section, the accuracy of the new polynomial shear strain function $f(z)$ is investigated. A simply supported-simply supported homogenous beam with Young's modulus of $E = 210 \text{ GPa}$, Poisson's ratio of $\nu = 0.3$ under concentrated force q_0 at the center of the beam is considered. The deflection of the mid-point of the present function is compared with Reddy's third-order shear deformation theory and also the exact solution obtained in [29].

The results in Table 2 are presented in a nondimensionalized form $\bar{w} = 10^3 wEI / q_0 L^3$. Where \bar{w} , w , q_0 , E , I and L are dimensionless deflection, normal deflection, point load, Young's modulus, second moment of inertia, and length of the beam, respectively.

The Equation 28 is used for calculation of percentage error in results in comparison with the exact elasticity solution:

$$\text{error} = \left(\frac{\text{value by numerical method} - \text{value by exact solution}}{\text{value by exact solution}} \right) \times 100\% \tag{28}$$

Table 2. Maximum dimensionless deflection for homogenous beam ($L/h = 2$)

Theory	nel=10	%Error	nel=20	%Error	nel=30	%Error	nel=40	%Error
Present	26.1117	4.8810	25.2847	1.5593	25.0112	0.4607	24.9006	0.0165
Reddy	26.3797	5.9575	25.5157	2.4871	25.1625	1.0684	25.0093	0.4531
Elasticity [29]	24.8965	0.00	24.8965	0.00	24.8965	0.00	24.8965	0.00

Where; nel indicates the number of elements used for beam mesh.

5. Numerical Results

In this section, FG beams are analyzed differently under various boundary conditions, including clamped-free (C-F), simply support-simply support (S-S), and clamped-clamped (C-C). For more detailed information on boundary conditions, Simsek (2010) [9] to be seen. Functionally graded material of beam is a composition of aluminum (AL) (as metal) and alumina (Al₂O₃) (as ceramic). Two different kinds of material are used for numerical analysis. The following material properties are used for numerical modeling. For bending and free vibration, material 1 from Ref. [16] is used. For buckling problems, material 2 from Kehya and Turan (2016) [8] is utilized.

$$\begin{aligned} \text{Material 1: } E_{Al} &= 70 \text{ GPa}, & \rho_{Al} &= 2700 \text{ kg/m}^3, & \nu_{Al} &= 0.23 \\ E_{Al_2O_3} &= 380 \text{ GPa}, & \rho_{Al_2O_3} &= 3800 \text{ kg/m}^3, & \nu_{Al_2O_3} &= 0.23 \\ \text{Material 2: } E_{Al} &= 70 \text{ GPa}, & \rho_{Al} &= 2702 \text{ kg/m}^3, & \nu_{Al} &= 0.3 \\ E_{Al_2O_3} &= 380 \text{ GPa}, & \rho_{Al_2O_3} &= 3960 \text{ kg/m}^3, & \nu_{Al_2O_3} &= 0.3 \end{aligned}$$

The properties alter according to the power-law. Thus, the upper surface is pure alumina, while the bottom surface is pure aluminum. The results of buckling analysis are compared with those available in Kehya and Turan (2016) [8]. Bending and free vibration results of FG beams are compared with those obtained and normalized from ANSYS solid 186 (see Figure 4). Simply supported condition for brick element gives inaccurate results; therefore, analyzing with simply support boundary condition is neglected. The FG beams are designed by solid 186 (20 nodes 3D element) with 20 layers. The cross-section mesh is 40×10 , and the length of the beam is meshed with 30 elements (see Figure 4-a).

5.1. Static Analysis

In this section, the bending behaviour of the FG beam under point load q_0 is investigated. For this analysis, the material one is used. The boundary condition is clamped-free, simply supported, and clamped-clamped. Tables 3 to 5 contain the dimensionless maximum deflection of FG beams. It can be observed that the results obtained by CBT are underestimated. The FSDBT results are good where the beam is deep, and the shear is dominant. HSDBT results are accurate enough in a different situation. The CBT has better results where the shear stress has not prevailed (slender beam). The maximum error values for the higher-order shear deformation results are less than seven percent when compared with ANSYS results. The new proposed function has better results in a fixed-fixed situation. The deflection of the FG beam is increased, by increasing in power-law index and porosities since the stiffness of FG beams is decreased.

Table 3. Maximum non-dimensional deflection ($\bar{w} = 10^3 w E_m I / q_0 L^3$) of C-F FGM beam under point load

L/h	Theory	$\alpha = 0$				$\alpha = 0.1$			$\alpha = 0.2$		
		n=0.2	n=1	n=2	n=5	n=0.2	n=1	n=2	n=0.2	n=1	n=2
5	ANSYS Solid 186	79.475	128.987	167.627	207.200	85.867	151.254	210.243	93.147	181.287	285.395
	CBT	74.553	123.074	157.986	187.241	80.426	143.015	197.189	87.323	171.904	269.566
	FSDBT	76.686	125.759	161.523	163.130	82.694	145.573	199.563	89.732	172.860	261.277
	HSDBT	76.735	126.288	162.357	194.192	82.727	146.523	202.148	89.760	175.780	275.309
	Present	76.681	126.212	162.285	194.185	82.669	146.439	202.068	89.698	175.686	275.215
20	ANSYS Solid 186	74.667	123.038	157.967	187.396	80.455	143.020	197.225	97.385	171.952	269.646
	CBT	74.553	123.074	157.986	187.241	80.426	143.015	197.189	87.323	171.904	269.566
	FSDBT	70.917	115.944	149.267	179.424	76.424	133.916	183.878	82.868	158.527	239.493
	HSDBT	74.739	123.348	158.353	187.807	80.623	143.314	197.606	87.531	172.235	270.049
	Present	74.731	123.336	158.337	187.785	80.615	143.301	197.587	87.523	172.221	270.027

Where; \bar{w} and w are dimensionless and normal deflection of the FG beams, respectively. E_m , I and L denote Young's modulus of the considered metal, second moment of inertia, and length of the FG beams, respectively. Also, q_0 indicates the point load.

Table 4. Maximum non-dimensional deflection ($\bar{w} = 10^3 w E_m I / q_0 L^3$) of S-S FGM beam under point load

L/h	Theory	$\alpha = 0$				$\alpha = 0.1$			$\alpha = 0.2$		
		n=0.2	n=1	n=2	n=5	n=0.2	n=1	n=2	n=0.2	n=1	n=2
5	CBT	4.659	7.692	9.873	11.702	5.027	8.938	12.323	5.458	10.743	16.864
	FSDBT	5.180	8.434	10.889	13.373	5.576	9.7237	13.368	6.039	11.494	17.361
	HSDBT	5.199	8.486	10.953	13.416	5.595	9.805	13.547	6.060	11.701	18.263
	Present	5.185	8.466	10.832	13.410	5.580	9.782	13.525	6.044	11.676	18.237
20	CBT	4.660	7.692	9.873	11.702	5.027	8.938	12.323	5.458	10.743	16.846
	FSDBT	4.455	7.280	9.376	11.292	4.800	8.407	11.545	5.205	9.948	15.029
	HSDBT	4.706	7.760	9.965	11.843	5.076	9.012	12.427	5.510	10.826	16.966
	Present	4.704	7.757	9.961	11.837	5.074	9.009	12.422	5.508	10.822	16.960

Table 5. Maximum non-dimensional deflection ($\bar{w} = 10^3 w E_m I / q_0 L^3$) of C-C FGM beam under point load

L/h	Theory	$\alpha = 0$				$\alpha = 0.1$			$\alpha = 0.2$		
		n=0.2	n=1	n=2	n=5	n=0.2	n=1	n=2	n=0.2	n=1	n=2
5	ANSYS Solid 186	1.618	2.576	3.416	4.4613	1.736	2.968	4.163	1.885	3.509	5.469
	CBT	1.165	1.923	2.468	2.925	1.257	2.234	3.080	1.364	2.685	4.209
	FSDBT	1.682	2.682	3.516	4.646	1.801	3.056	4.237	1.941	3.563	5.372
	HSDBT	1.692	2.698	3.519	4.590	1.812	3.081	4.273	1.953	3.621	5.591
	Present	1.676	2.675	3.495	4.576	1.795	3.055	4.246	1.935	3.592	5.559
20	ANSYS Solid 186	1.193	1.969	2.523	3.019	1.286	2.275	3.150	1.397	2.742	4.287
	CBT	1.165	1.923	2.467	2.925	1.257	2.234	3.080	1.364	2.685	4.209
	FSDBT	1.137	1.854	2.391	2.901	1.224	2.138	2.939	1.327	2.527	3.817
	HSDBT	1.211	1.990	2.558	3.064	1.305	2.308	3.183	1.416	2.767	4.326
	Present	1.209	1.987	2.554	3.059	1.303	2.304	3.178	1.414	2.763	4.323

5.2. Buckling analysis

In the following section (Table 6), the buckling behaviour of the FG beam is studied by assuming material 2 (see Kehya and Turan (2016) [8]). For buckling analysis, the following stability equation ($[K] - N_{cr}[K_G]) u = 0$ is solved. The first three dimensionless critical buckling load of the FG beam is extracted. The critical buckling load of clamped-clamped FG beams by various power-law and the length-to-depth ratio is investigated. The results are compared with those available and obtained by Kehya and Turan (2016) [8]. The FSDBT results are overestimated where the beam is slender ($L/h = 20$), whereas, the CBT results are overestimated when the beam is thick ($L/h = 5$). Both higher-order shear deformation theories have accurate results when compared with those available in Kehya and Turan (2016) [8].

An obvious outcome here is that the results of the proposed model are approximately close to the results of Kehya and Turan (2016) [8]. Maximum differences of higher-order shear deformation results are almost five percent. By increasing the power-law index, the differences are increased. Increasing in Both power-law and porosity exponent has a significant effect on buckling loads. The buckling load decreases when the power-law and porosities are increased.

Table 6. The non-dimensional first three buckling critical loads ($\bar{N}_{cr} = N_{cr}L^2 / E_m I$) of C-C FG beam

L/h	\bar{N}_{cr}	Theory	$\alpha = 0$				$\alpha = 0.1$			$\alpha = 0.2$		
			n=0.2	n=1	n=2	n=5	n=0.2	n=1	n=2	n=0.2	n=1	n=2
5	1	[8]	-	79.3903	61.7449	49.5828	-	-	-	-	-	-
		CBT	156.791	94.608	72.704	60.095	145.382	81.416	58.131	133.944	67.733	42.407
		FSDBT	122.479	79.691	60.919	46.568	119.076	69.895	50.482	110.556	59.893	39.718
		HSDBT	127.641	79.620	60.901	46.829	119.266	69.694	50.072	110.757	59.224	38.119
	2	Present	127.864	79.748	60.938	46.682	119.469	69.800	50.097	110.939	59.307	38.139
		CBT	287.258	172.778	131.309	106.785	266.418	148.685	401.819	245.525	123.696	76.299
		FSDBT	193.962	123.538	93.138	66.931	182.131	109.630	78.566	170.026	95.254	63.290
		HSDBT	194.614	123.865	93.672	68.147	182.774	109.711	78.387	170.647	94.664	61.425
	3	Present	195.604	124.454	93.968	97.999	183.684	110.209	78.612	171.476	95.069	61.592
		CBT	470.089	281.448	210.651	167.651	436.128	242.193	167.775	402.079	201.478	121.755
		FSDBT	278.509	180.051	134.246	92.070	262.608	161.320	114.872	246.225	141.797	94.370
		HSDBT	281.249	181.865	136.205	94.912	265.226	162.655	115.616	248.709	142.157	92.818
20	1	Present	283.280	183.143	136.935	94.848	267.087	163.748	116.193	250.402	143.062	93.265
		[8]	-	-	-	-	-	-	-	-	-	-
		CBT	175.350	106.189	82.643	69.628	162.547	91.382	66.203	149.713	76.025	48.418
		FSDBT	182.218	111.045	86.140	71.138	168.294	96.275	70.064	155.334	81.448	53.921
	2	HSDBT	172.577	104.795	81.511	68.215	160.082	90.309	65.446	147.542	75.260	48.028
		Present	172.595	104.805	81.511	68.189	160.099	90.317	65.446	147.556	75.266	48.028
		CBT	356.277	215.702	167.711	141.084	330.271	185.627	134.330	304.202	154.433	98.226
		FSDBT	360.633	221.589	171.547	140.211	335.178	192.421	139.890	309.615	163.091	107.999
	3	HSDBT	342.680	208.760	162.091	134.323	318.137	180.224	130.503	293.469	150.523	96.168
		Present	342.866	208.863	162.145	134.274	318.304	180.306	130.541	293.617	150.585	96.193
		CBT	687.887	416.237	323.036	271.005	637.700	358.196	258.663	587.389	297.996	189.065
		FSDBT	679.597	419.084	323.580	260.927	632.282	364.704	264.763	584.681	309.871	205.264
3	HSDBT	647.076	395.596	306.396	250.790	601.343	342.237	247.477	555.297	286.575	183.254	
	Present	647.355	395.747	306.410	250.464	601.594	342.360	247.482	555.522	286.669	183.262	

Where; \bar{N}_{cr} and N_{cr} are dimensionless and normal critical buckling load of the FG beams, respectively. E_m , I and L denote young's modulus of the considered metal, second moment of inertia, and length of the FG beams, respectively.

5.3. Free Vibration

The first three dimensionless frequencies $\bar{\omega}$ of C-F, S-S, and C-C of FG and PFG beams are illustrated in Tables 7 to 9, respectively. Various boundary conditions, length-to-depth ratio (L/h) are considered. The effect of different values of the power-law index n and porosity index α on the vibration characteristic of the FG beams is investigated. For free vibration analysis, the following eigen-value equation ($[K]-\omega^2[M] u = 0$) is solved [30-32]. The results of different theories are compared with those obtained from ANSYS solid 186. The CBT overestimates the frequencies due to the neglect of shear deformation. The FSDBT loses accuracy when the FG beams become slender.

In most cases, results obtained from higher-order shear deformation theories have less than one percent differences in comparison with those obtained from ANSYS. The maximum difference in results is less than five percent. The results of the new proposed shear deformation have less difference with ANSYS when the FG beams become slender. By increasing in porosities, the FG beam vibrations decrease. An increase in the power-law index n , leads to decreasing the values of frequencies. While the power-law index tends to zero (full-ceramic), the frequency values are increased. The first three mode shapes of FG beams are plotted in Figure 4-b for clamped-clamped FG beams of ($L/h = 5$), $n = 1$ and $\alpha = 0.0$.

Table 7. The first three non-dimensional frequencies ($\bar{\omega} = \omega L^2 \rho_{eq}^{0.5} / h E_{eq}^{0.5}$) of C-F FGM beam

L/h	$\bar{\omega}_i$	Theory	$\alpha = 0$				$\alpha = 0.1$			$\alpha = 0.2$		
			n=0.2	n=1	n=2	n=5	n=0.2	n=1	n=2	n=0.2	n=1	n=2
1		ANSYS Solid 186	0.9691	0.9131	0.9162	0.9877	0.9657	0.8868	0.8715	0.9394	0.8630	0.8152
		CBT	0.9832	0.9240	0.9285	1.0176	0.9923	0.9034	0.8786	1.0031	0.8738	0.7988
		FSDBT	0.9629	0.9085	0.9123	0.9931	0.9609	0.8905	0.8804	0.9585	0.8671	0.8348
		HSDBT	0.9624	0.9065	0.9099	0.9907	0.9717	0.8873	0.8626	0.9828	0.8595	0.7875
		Present	0.9629	0.9069	0.9103	0.9908	0.9722	0.8877	0.8629	0.9833	0.8598	0.7877
5	2	ANSYS Solid 186	5.2826	5.0152	4.9685	5.2396	5.2752	4.8817	4.7433	5.1459	4.7741	4.4838
		CBT	5.8985	5.5139	5.5082	6.0088	5.9527	5.3856	5.1976	6.0175	5.2023	4.7132
		FSDBT	5.2451	4.9719	4.9412	5.2051	5.2454	4.8982	4.8072	5.2440	4.7985	4.6055
		HSDBT	5.2270	4.9529	4.9298	5.2148	5.2880	4.8677	4.6986	5.3592	4.7391	4.3261
		Present	5.2437	4.9666	4.9407	5.2196	5.3047	4.8806	4.7080	5.3760	4.7508	4.3336
3		ANSYS Solid 186	7.8880	7.9937	7.9145	9.9068	7.8787	7.8466	8.8496	7.6840	7.8908	7.9016
		CBT	7.8603	7.8873	7.9151	7.9376	7.9524	7.8932	7.8227	8.0633	7.9006	7.7021
		FSDBT	7.8589	7.8713	7.8834	7.8860	7.8590	7.8698	7.8800	7.8590	7.8679	7.8754
		HSDBT	7.8588	7.8704	7.8817	7.8857	7.9508	7.8736	7.7822	8.0615	7.8774	7.6512
		Present	7.8588	7.8708	7.8821	7.8858	7.9505	7.8741	7.7826	8.0615	7.8780	7.6518
1		ANSYS Solid 186	0.9911	0.9319	0.9366	1.0264	0.9878	0.9081	0.8999	0.9847	0.8808	0.8330
		CBT	0.9903	0.9312	0.9364	1.0267	0.9994	0.9106	0.8864	1.0103	0.8809	0.8075
		FSDBT	1.0149	0.9590	0.9629	1.0481	1.0129	0.9404	0.9301	1.0106	0.9170	0.8836
		HSDBT	0.9884	0.9296	0.9347	1.0243	0.9975	0.9091	0.8850	1.0084	0.8796	0.8064
		Present	0.9885	0.9297	0.9348	1.0244	0.9976	0.9092	0.8851	1.0085	0.8797	0.8064
20	2	ANSYS Solid 186	6.1451	5.7819	5.8058	6.3438	6.1040	5.6366	5.5808	6.1083	5.4697	5.1703
		CBT	6.1884	5.8181	5.8491	6.4120	6.2453	5.6889	5.5362	6.3133	5.5034	5.0421
		FSDBT	6.2953	5.9517	5.9710	6.4796	6.2846	5.8403	5.7714	6.2715	5.6965	5.4877
		HSDBT	6.1078	5.7505	5.7782	6.3117	6.1656	5.6268	5.4752	6.2346	5.4480	4.9949
		Present	6.1112	5.7535	5.7814	6.3155	6.1689	5.6295	5.4779	6.2378	5.4503	4.9971
3		ANSYS Solid 186	16.9269	15.9399	15.9838	17.3895	16.8802	15.5482	15.3759	16.8344	15.0983	14.2623
		CBT	17.2489	2116	16.2909	17.8537	17.4075	15.8508	15.4162	17.5970	15.3324	14.0354
		FSDBT	17.3541	16.4194	16.4514	17.7714	17.3295	16.1228	15.9186	17.2986	15.7830	15.1563
		HSDBT	16.7361	15.7817	15.8412	17.2229	16.9008	15.4547	15.0285	17.0962	14.9790	13.7352
		Present	16.7572	15.8002	15.8611	17.2467	16.9213	15.4716	15.0458	17.1162	14.9940	13.7490

Where; $\bar{\omega}$ and ω are dimensionless and normal frequency of the FG beams. ρ_{eq} , E_{eq} and h denote equal density, equal Young's modulus of FG beams, and height of the FG beams, respectively.

Table 8. The first three non-dimensional frequencies ($\bar{\omega} = \omega L^2 \rho_{eq}^{0.5} / h E_{eq}^{0.5}$) of S-S FGM beam

L/h	$\bar{\omega}_i$	Theory	$\alpha = 0$				$\alpha = 0.1$			$\alpha = 0.2$		
			n=0.2	n=1	n=2	n=5	n=0.2	n=1	n=2	n=0.2	n=1	n=2
5	1	CBT	2.7353	2.5554	2.5555	2.7978	2.7602	2.4948	2.4099	2.7900	2.4082	2.1824
		FSDBT	2.6264	2.4813	2.4864	2.6866	2.6222	2.4347	2.4037	2.6171	2.3741	2.2843
		HSDBT	2.6184	2.4597	2.4566	2.6559	2.6448	2.4073	2.3260	2.6760	2.3310	2.1192
		Present	2.6209	2.4917	2.4581	2.6558	2.6474	2.4092	2.3272	2.6786	2.3327	2.1201
2		CBT	7.8368	7.5908	7.4450	7.5565	7.9249	7.5061	7.1567	8.0306	7.3695	6.6629
		FSDBT	7.8568	4.8469	7.8380	7.8298	7.8571	7.8474	7.8384	7.8574	7.8479	7.8369
		HSDBT	7.8270	7.4927	7.3113	7.4287	7.9137	7.3890	6.9986	8.0175	7.2287	6.4864
		Present	7.8273	7.4955	7.3138	7.4288	7.9140	7.3922	7.0014	8.0180	7.2326	6.4896

3	CBT	10.4797	10.0092	10.1267	10.9471	10.5791	8.8515	9.7208	10.6982	9.6369	9.1275	
	FSDBT	9.2071	8.7465	8.6968	9.1405	9.2097	8.6203	8.4656	8.2094	8.4490	8.1181	
	HSDBT	9.1507	8.9266	8.9957	9.3625	9.2640	8.8603	8.7422	9.3966	8.7600	8.3490	
	Present	9.1779	8.9476	9.0108	9.3648	9.2915	8.8798	8.7548	9.4242	8.7775	8.3584	
1	CBT	2.7783	2.6116	2.6255	2.8785	2.8038	2.5535	2.4849	2.8343	2.4701	2.2629	
	FSDBT	2.8440	2.6877	2.6982	2.9353	2.8387	2.6364	2.6066	2.8324	2.5704	2.4767	
	HSDBT	2.7669	2.6021	2.6155	2.8643	2.7625	2.5448	2.4763	2.8232	2.4623	2.2563	
	Present	2.7674	2.6025	2.6160	2.8649	2.793	2.5452	2.4767	2.8236	2.4626	2.2566	
20	2	CBT	11.0782	10.4013	10.4456	11.4489	11.1797	10.1670	9.8792	11.3011	9.8307	8.9866
		FSDBT	11.2593	10.6461	10.6785	11.5799	11.2406	10.4479	10.3233	11.2177	10.1920	9.8179
	3	HSDBT	10.9023	10.2550	10.2930	11.2333	11.0061	10.0325	9.7482	11.1296	9.7112	8.8860
		Present	10.9095	10.2612	10.2997	11.2413	11.0131	10.0382	9.7540	11.1364	9.7162	8.8905
3	CBT	24.7892	23.1754	23.1896	25.3285	25.0148	22.6354	21.8957	25.2843	21.8656	19.8772	
	FSDBT	24.9194	23.5821	23.6216	25.4905	24.8857	23.1598	22.8622	24.8431	22.6114	21.7740	
	HSDBT	23.9478	22.4933	22.4961	24.3855	24.1839	22.0108	21.3048	24.4636	21.3123	19.4260	
	Present	23.9814	22.5219	22.5261	24.4201	24.2166	22.0368	21.3306	24.4955	21.3352	19.4462	

Table 9. The first three non-dimensional frequencies ($\bar{\omega} = \omega L^2 \rho_{eq}^{0.5} / h E_{eq}^{0.5}$) of C-C FGM beam

L/h	$\bar{\omega}_i$	Theory	$\alpha = 0$				$\alpha = 0.1$			$\alpha = 0.2$		
			n=0.2	n=1	n=2	n=5	n=0.2	n=1	n=2	n=0.2	n=1	n=2
1	1	ANSYS Solid 186	5.2299	5.0122	4.9606	5.1645	5.2246	4.8845	4.7686	5.0965	4.7968	4.5411
		CBT	6.1801	5.8020	5.8230	6.3775	6.2369	5.6715	5.5063	6.3409	5.4841	5.0075
		FSDBT	5.1690	4.9400	4.9115	5.1012	5.1747	4.8779	4.7958	5.1789	4.7915	4.6168
		HSDBT	5.1489	4.9215	4.9054	5.1277	5.2145	4.8534	4.7048	5.2905	4.7463	4.3745
		Present	5.1734	4.9422	4.9221	5.1355	5.2390	4.8730	4.7194	5.3152	4.7643	4.3865
5	2	ANSYS Solid 186	12.1074	11.7140	11.4841	11.6668	12.1230	11.4455	11.1008	11.8573	11.3048	10.6935
		CBT	15.7035	15.0231	14.9322	15.5251	15.8840	14.6923	14.1313	16.1004	14.2045	12.8297
		FSDBT	11.9607	11.4979	11.3338	11.4483	11.9981	11.4109	11.1529	12.0330	11.2767	10.8481
		HSDBT	11.9336	11.4851	11.3785	11.6231	12.1065	11.3731	10.9769	12.3056	11.1822	10.3056
		Present	12.0301	11.5688	11.4883	11.6646	12.2037	11.4530	11.0395	12.4037	11.2569	10.3589
3	3	ANSYS Solid 186	15.8091	15.9454	15.7048	15.6509	15.7821	15.6291	15.4867	15.3895	15.6826	15.5109
		CBT	16.2039	15.8352	15.9141	16.7125	16.3563	15.8150	15.6505	16.5394	15.8006	15.3448
		FSDBT	15.7139	15.6698	15.6219	15.5824	15.7146	15.6731	15.6261	15.7154	15.6767	15.6301
		HSDBT	15.7137	15.6649	15.6108	15.5805	15.8970	15.6547	15.3655	16.1175	15.6399	15.0336
		Present	15.7139	15.6668	15.6125	15.5805	15.8972	15.6571	15.3672	16.1178	15.6427	15.0351
1	1	ANSYS Solid 186	6.2311	5.8673	5.8906	6.4264	6.2118	5.7199	5.6636	6.1924	5.5513	5.2501
		CBT	6.2967	5.9212	5.9541	6.5278	6.3545	5.7900	5.6364	6.4237	5.6015	5.1345
		FSDBT	6.3744	6.0303	6.0491	6.5537	6.3642	5.9188	5.8492	6.3516	5.7747	5.5644
		HSDBT	6.1725	5.8170	5.8448	6.3736	6.2319	5.6941	5.5422	6.3025	5.5160	5.0615
		Present	6.1777	5.8215	5.8497	6.3795	6.2369	5.6982	5.5464	6.3074	5.5197	5.0649
20	2	ANSYS Solid 186	16.8496	15.8869	15.9253	17.2788	16.8038	15.5003	15.3290	16.7576	15.0584	14.2358
		CBT	17.2974	16.2632	16.3491	17.9206	17.4564	15.9025	15.4748	17.6465	15.3842	14.0937
		FSDBT	17.2512	16.3402	16.3678	17.6296	17.2301	16.0519	15.8488	17.2027	15.6767	15.1031
		HSDBT	16.5823	15.6619	15.7197	17.0411	16.7496	15.3480	14.9310	16.9476	14.8887	13.6713
		Present	16.6113	15.6876	15.7475	17.0742	16.7881	15.3715	14.9552	16.9754	14.9096	13.6906
3	3	ANSYS Solid 186	32.2322	304377	304549	32.8330	32.1582	29.7249	29.3529	32.0838	28.9112	27.3173
		CBT	3.7305	31.7045	31.8574	34.9081	34.0407	30.9996	30.1469	34.4116	29.9868	27.4467
		FSDBT	33.0417	31.3410	31.3388	33.5249	33.0158	30.8199	30.3948	32.9786	30.1353	29.0245
		HSDBT	31.4829	29.8095	29.8814	32.1783	31.8173	29.2491	28.4363	32.2112	28.4196	26.1139
		Present	31.5721	29.8885	29.9664	32.2779	31.9043	29.3217	28.5107	32.2961	28.4830	26.1737

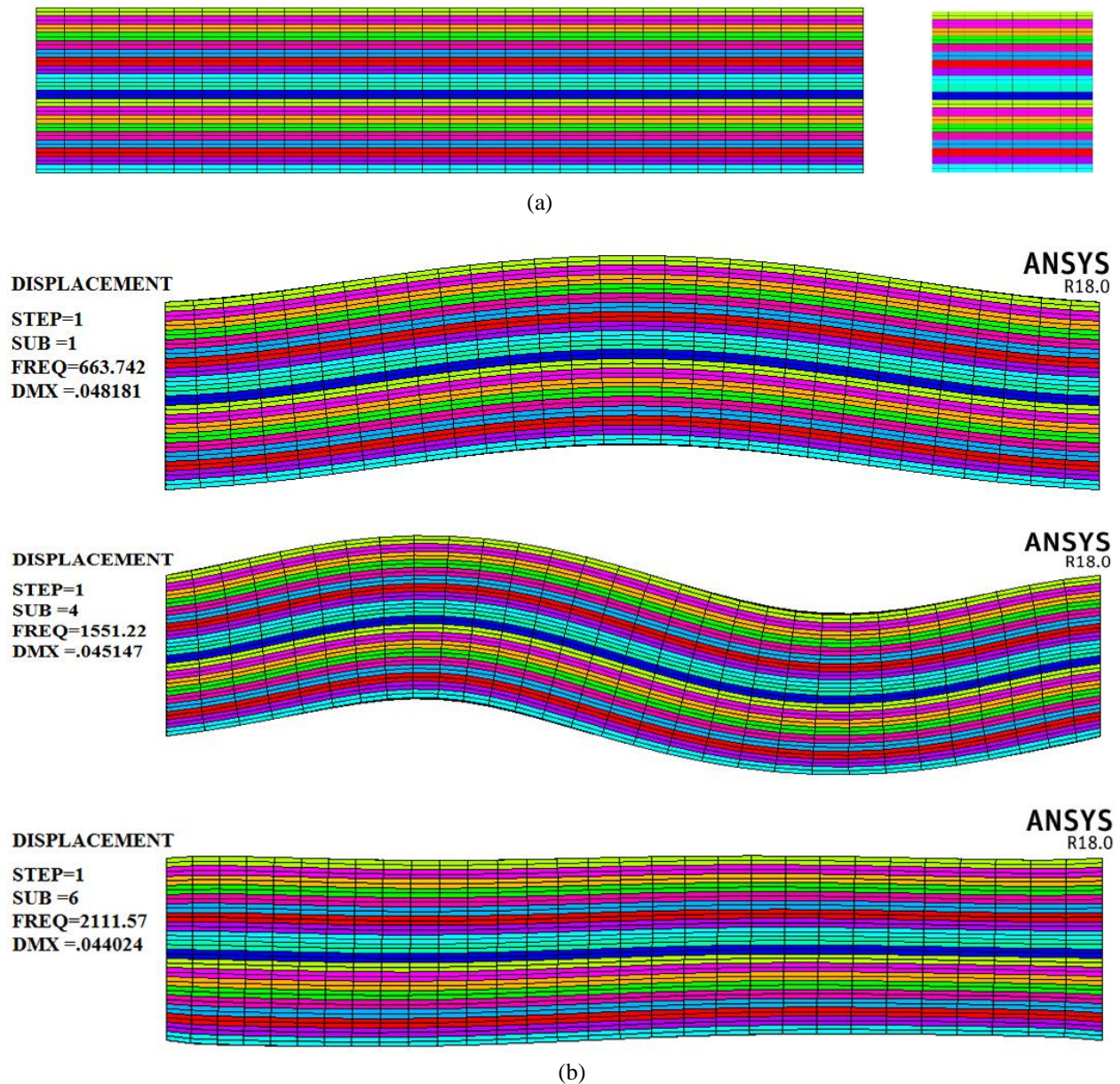


Figure 4. (a) FG beam mesh in ANSYS (b) Three first mode of FG beams from ANSYS ($L/h = 5, n = 1, \alpha = 0$)

6. Conclusions

In the present paper, static, buckling and free vibration of various FG beams by various beam theories are studied. Hamilton’s principle is used for acquiring the equation of motion. Different boundary conditions, power-law index, and porosity conditions are assumed for estimating the behaviour of FG beams. The shift of the neutral axis position is taken into account in the analysis. A new polynomial function is introduced for approximating the shear strain along with the thickness. For validation of the results of the free vibration and bending results, FG beams are modeled in ANSYS (solid 186). The results specify the influences of the slenderness ratio (L/h), material distribution, porosity index, on the characteristics of the beam as follow:

- The proposed shear strain function satisfies the stress-free boundary condition on the bottom and top surface of the beam. The numerical results show that significant accuracies can be reached using the new proposed shear-strain function. Therefore, the shear correction factors do not require, which is common in classic beam theories;
- By increasing in slenderness ratio (L/h), the deflection, natural frequencies, and critical buckling load are increased, respectively;
- Non-dimensional frequencies increase with a decrease in power-law and porosity index;
- The stiffness of the FG beam is following a decreasing pattern by increasing the porosity and power-law index. Therefore, the deflection increases, while the critical buckling load is decreased;

- The CBT bending results is underestimated, while the buckling and free vibration results are overestimated, especially in the thick beam;
- The FSDBT results are less inaccurate when the results are compared with HSDBT and ANSYS results. Due to the dependency of a shear correction factor to the power-law index, obtaining various shear correction factor is unendurable;
- Both HSDBTs have accurate results when the results are compared with ANSYS results. The proposed model has less error, especially when the beam becomes slender. Therefore, the proposed function can be used in practical applications to obtain more accurate results.

7. Conflicts of Interest

The authors declare no conflict of interest.

8. References

- [1] Sinha, Gourav P., and Kumar, Bipin. "Review on Vibration Analysis of Functionally Graded Material Structural Components with Cracks." *Journal of Vibration Engineering & Technologies* (April 2020): 1-27. doi:10.1007/s42417-020-00208-3.
- [2] Xia, You-Ming, Li, Shi-Rong, and Wan, Ze-Qing. "Bending Solutions of FGM Reddy–Bickford Beams in Terms of those of the Homogenous Euler–Bernoulli Beams." *Acta Mechanica Solida Sinica* 32, No. 4 (August 2019): 499-516. doi:10.1007/s10338-019-00100-y.
- [3] Abbasnejad, Behrokh, Rezazadeh, Ghader, and Shabani, Rasool. "Stability Analysis of a Capacitive FGM Micro-Beam using Modified Couple Stress Theory." *Acta Mechanica Solida Sinica* 26, No. 4 (August 2013): 427-440. doi:10.1016/S0894-9166(13)60038-5.
- [4] Li, Shirong, Wang, Xuan, and Wan, Zeqing. "Classical and Homogenized Expressions for Buckling Solutions of Functionally Graded Material Levinson Beams." *Acta Mechanica Solida Sinica* 28, No. 5 (October 2015): 592-604. doi:10.1016/S0894-9166(15)30052-5.
- [5] Coskun, Semsı, Kim, Jinseok, and Toutanji, Houssam. "Bending, Free Vibration, and Buckling Analysis of Functionally Graded Porous Micro-Plates using a General Third-Order Plate Theory." *Journal of Composites Science* 3, No. 1 (February 2019): 1-22. doi:10.3390/jcs3010015.
- [6] Alshorbagy, Amal E., Eltaher, Mohamed A., and Mahmoud, Fatin. "Free Vibration Characteristics of a Functionally Graded Beam by Finite Element Method." *Applied Mathematical Modelling* 35, No. 1 (January 2011): 412-425. doi:10.1016/j.apm.2010.07.006.
- [7] Adámek, Vitezslav, and Valeš, Frantisek. "Analytical Solution for a Heterogeneous Timoshenko Beam Subjected to an Arbitrary Dynamic Transverse Load." *European Journal of Mechanics - A/Solids* 49 (January 2015): 373-381. doi:10.1016/j.euromechsol.2014.07.016.
- [8] Kahya, Volkan, and Turan, Muhittin. "Finite Element Model for Vibration and Buckling of Functionally Graded Beams based on the First-Order Shear Deformation Theory." *Composites Part B: Engineering* 109 (January 2017): 108-115. doi:10.1016/j.compositesb.2016.10.039.
- [9] Şimşek, Mesut. "Fundamental Frequency Analysis of Functionally Graded Beams by using Different Higher-Order Beam Theories." *Nuclear Engineering and Design* 240, No. 4 (April 2010): 697-705. doi:10.1016/j.nucengdes.2009.12.013.
- [10] Sankar, Bhavani V. "An Elasticity Solution for Functionally Graded Beams." *Composites Science and Technology* 61, No. 5 (April 2001): 689-696. doi:10.1016/S0266-3538(01)00007-0.
- [11] Eltaher, Mohamed A, Alshorbagy, Amal E, and Mahmoud, Fatin. "Determination of Neutral Axis Position and Its Effect on Natural Frequencies of Functionally Graded Macro/Nanobeams." *Composite Structures* 99 (May 2013): 193-201. doi:10.1016/j.compstruct.2012.11.039.
- [12] Li, Shi-Rong, and Batra, Romesh C. "Relations between Buckling Loads of Functionally Graded Timoshenko and Homogeneous Euler–Bernoulli Beams." *Composite Structures* 95 (January 2013): 5-9. doi:10.1016/j.compstruct.2012.07.027.
- [13] Lee, Jung Woo, and Lee, Jung Youn. "Free Vibration Analysis of Functionally Graded Bernoulli-Euler Beams using an Exact Transfer Matrix Expression." *International Journal of Mechanical Sciences* 122 (March 2017): 1-17. doi:10.1016/j.ijmecsci.2017.01.011.
- [14] Şimşek, Mesut. "Bi-Directional Functionally Graded Materials (BDFGMs) for Free and Forced Vibration of Timoshenko Beams with Various Boundary Conditions." *Composite Structures* 133 (December 2015): 968-978. doi:10.1016/j.compstruct.2015.08.021.

- [15] Jing, Li-Long, Ming, Ping-Jian, Zhang, Wen-Ping, Fu, Li-Rong, and Cao, Yi-Peng. "Static and Free Vibration Analysis of Functionally Graded Beams by Combination Timoshenko Theory and Finite Volume Method." *Composite Structures* 138 (March 2016): 192-213. doi:10.1016/j.compstruct.2015.11.027.
- [16] Pradhan, Karan Kumar, and Chakraverty, Snehashish. "Effects of Different Shear Deformation Theories on Free Vibration of Functionally Graded Beams." *International Journal of Mechanical Sciences* 82 (May 2014): 149-160. doi:10.1016/j.ijmecsci.2014.03.014.
- [17] Giunta, Gaetano, Belouettar, Salim, and Ferreira, Antonio J.M. "A Static Analysis of Three-Dimensional Functionally Graded Beams by Hierarchical Modelling and a Collocation Meshless Solution Method." *Acta Mechanica* 227 (December 2015): 969-991. doi:10.1007/s00707-015-1503-3.
- [18] Frikha, Ahmed, Hajlaoui, Abdessalem, Wali, Mondher, and Dammak, Fakhreddine. "A New Higher Order C0 Mixed Beam Element for FGM Beams Analysis." *Composites Part B: Engineering* 106 (December 2016): 181-189. doi:10.1016/j.compositesb.2016.09.024.
- [19] Patil, Mukund A., and Kadoli, Ravikiran. "Differential Quadrature Solution for Vibration Control of Functionally Graded Beams with Terfenol-D Layer." *Applied Mathematical Modelling* 84 (August 2020): 137-157. doi:10.1016/j.apm.2020.03.035.
- [20] Pham, Hoang-Anh, Truong, Viet-Hung, and Tran, Minh-Tu. "Fuzzy Static Finite Element Analysis for Functionally Graded Structures with Semi-Rigid Connections." *Structures* 26 (August 2020): 639-650. doi:10.1016/j.istruc.2020.04.036.
- [21] Mohammed, Douaa Raheem, and Ismael, Murtada A. "Effect of Semi-Rigid Connection on Post-Buckling Behaviour of Frames using Finite Element Method." *Civil Engineering Journal* 5, No. 7 (July 2019) 1619-1630. doi:10.28991/cej-2019-03091358.
- [22] Rahgozar, Peyman. "Free Vibration of Tall Buildings using Energy Method and Hamilton's Principle." *Civil Engineering Journal* 6, No. 5 (May 2020) 945-953. doi:10.28991/cej-2020-03091519.
- [23] Kamgar, Reza, and Rahgozar, Reza. "Determination of Optimum Location for Flexible Outrigger Systems in Non-Uniform Tall Buildings using Energy Method." *International Journal of Optimization in Civil Engineering* 5, No. 4 (January 2015): 433-444.
- [24] Tavakoli, Reihaneh, Kamgar, Reza, and Rahgozar, Reza. "Seismic Performance of Outrigger-Belt Truss System Considering Soil-Structure Interaction." *International Journal of Advanced Structural Engineering* 11 (March 2019): 45-54. doi:10.1007/s40091-019-0215-7.
- [25] Elishakoff, Isaac, Pentaras, Demetris, and Gentilini, Cristina. "Mechanics of Functionally Graded Material Structures." (December 2015). doi:10.1142/9505.
- [26] Heidarzadeh, Heisam, and Kamgar, Reza. "Evaluation of the Importance of Gradually Releasing Stress around Excavation Regions in Soil Media and the Effect of Liners Installation Time on Tunneling." *Geotechnical and Geological Engineering* 38 (April 2020): 2213-2225. doi:10.1007/s10706-019-01158-8.
- [27] Heidarzadeh, Heisam, and Kamgar, Reza. "Necessity of Applying the Concept of the Steady State on the Numerical Analyses of Excavation Issues: Laboratory, Field and Numerical Investigations." *Geomechanics and Geoengineering* 1 (May 2020): 1-13. doi:10.1080/17486025.2020.1755466.
- [28] Tavakoli, Reihaneh, Kamgar, Reza, and Rahgozar, Reza. "Seismic Performance of Outrigger-Braced System based on Finite Element and Component-Mode Synthesis Methods." *Iranian Journal of Science and Technology - Transactions of Civil Engineering* (July 2019). doi:10.1007/s40996-019-00299-3.
- [29] Ghugal, Yuwaraj M., and Sharma, Rajneesh. "A Refined Shear Deformation Theory for Flexure of Thick Beams." *Latin American Journal of Solids and Structures* 8, No. 2 (June 2011): 183-195. doi:10.1590/S1679-78252011000200005
- [30] Heidari, Ali, Rahgozar, Reza, and Kamgar, Reza. "Free Vibration Analysis of Tall Building with Geometrical Discontinuities." *Asian Journal of Civil Engineering* 15, No. 1 (January 2014): 107-122.
- [31] Kamgar, Reza, and Rahgozar, Reza. "A Simple Approximate Method for Free Vibration Analysis of Framed Tube Structures." *The Structural Design of Tall and Special Buildings* 22 (February 2013): 217-234. doi:10.1002/tal.680.
- [32] Kamgar, Reza, and Saadatpour, Mohammad M. "A Simple Mathematical Model for Free Vibration Analysis of Combined System Consisting of Framed Tube, Shear core, Belt truss and Outrigger System with Geometrical Discontinuities." *Applied Mathematical Modelling* 36, No. 10 (October 2012): 4918-4930. doi:10.1016/j.apm.2011.12.029.